Utilizing Mobile Energy Storage Systems as Potential Enhancements of Renewable Energy Hosting Capacity for Distribution Systems

Xiaochuan Liu, Hailiang Lu, Bochao Yang, Zhitong Tian, Lei Lan
School of Electrical Engineering and Automation
Wuhan University
Wuhan, China
{xiaochuan.liu, luhailiang, yangbochao2022, 2020302191011, lanlei}@whu.edu.cn

***Abstract*—As renewable energy sources (RESs) are continuously integrated into the existing power systems, enhancing the system RES hosting capacity (HC) is crucial for the existing distribution systems. Mobile energy storage systems (MESSs) have the potential to enhance RES HC considering their spatiotemporal flexibilities. To utilize MESSs as RES HC enhancements, a time-space-network-based MESS scheduling model is proposed to describe the detailed MESS spatiotemporal behaviors, where the MESS scheduling decisions are depicted using arc-related variables. To assess the enhanced system HC, an optimal-power-flow-based RES HC evaluation model is proposed for integrated MV-LV networks. The problem is formulated as a mixed-integer second-order cone programming model, which aims to find the maximum HC with the consideration of system operational constraints. The proposed model is verified using an integrated test system with the Sioux Falls transportation network, a 33-bus distribution system and three 18-bus distribution systems. The results demonstrate the effectiveness of utilizing MESSs as RES HC enhancements, highlighting their technical potential under policy-driven renewable-integration requirements.**

***Index Terms*— Mobile energy storage, hosting capacity, renewable energy sources, spatiotemporal flexibility.**

I. Introduction

As fossil fuel reserves continue to decline and the global environmental crisis worsens, there is an increasing urgency to shift toward sustainable energy resources [1]. Over the past few decades, the existing distribution systems have witnessed a continuous integration of renewable energy sources (RESs) such as photovoltaic (PV) panels and wind turbines (WTs) [2]. Besides environmental and economic benefits, the increasing RES penetration level has also introduced non-negligible challenges to power systems, such as voltage rise, increased feeder losses, and the overloading of both transmission lines and transformers [3], [4]. These challenges have emerged as the primary barrier to the further integration of new RESs within distribution networks. Therefore, it is of urgent need to effectively evaluate the capability of the existing distribution systems to integrate new RESs without requiring infrastructure upgrades or violating any operational constraints.

To address these challenges, the concept of hosting capacity (HC) was proposed [5], which is defined as the maximum amount of power generation that a system can host without violating any operational performance limits given the existing system infrastructure. Nowadays, besides simply assessing the HC, enhancing the system RES HC is gradually becoming another important goal for distribution system operators (DSOs) [6]. Various hosting capacity enhancement methods, e.g., voltage control, active power curtailment [7], energy storage systems (ESSs) [8]-[10], have been studied in recent publications. Among all these different solutions, utilizing ESSs to improve system HC is promising and have been attracting attention in recent years. For instance, in [8], an optimal operation scheme of ESSs for load and distributed generation HC improvement is proposed. In [9], the authors propose an optimal allocation and sizing method for ESSs to increase PV HC, while considering network reinforcement and capacitor bank allocation. An optimal ESS planning and placement scheme is introduced in [10], where simultaneous active and reactive power control is included for further PV HC enhancement.

While the aforementioned studies only incorporate static ESSs, given the rising trend of adopting mobile energy storage systems (MESSs) into distribution system operation [11], and considering their superior operational flexibilities due to the spatiotemporal mobility, it is promising to also harness the flexibility of MESSs for further RES HC enhancement. Only a few publications consider utilizing MESSs to improve RES HC. In [12], a collaborative scheduling scheme including both network reconfiguration and MESSs is proposed to achieve maximized system HC. However, only an over-simplified MESS scheduling model is presented while the authors fail to describe the detailed temporal-spatial behaviors of MESSs. Moreover, most of the literature only focuses on analyzing RES HC for distribution systems with only one voltage level, e.g., only LV networks. As distribution systems with different voltage levels are naturally coupled, it is essential to also include an integrated MV-LV distribution system model during HC assessment.

In this context, this paper aims to bridge the gap in utilizing MESSs as potential RES HC enhancements. A detailed MESS scheduling model describing its spatiotemporal behaviors is introduced, which is then integrated into an optimal power flow (OPF) based RES HC evaluation model for integrated medium-voltage (MV) and low-voltage (LV) distribution networks to verify the effectiveness of MESSs serving as a HC enhancement method. The optimization problem is formulated as a mixed-integer second-order cone programming (MISOCP)

This work was supported by the National Natural Science Foundation of China under Grant 52307140, in part by the China Postdoctoral Science Foundation under Grant 2025M770487.

979-8-3315-6138-1

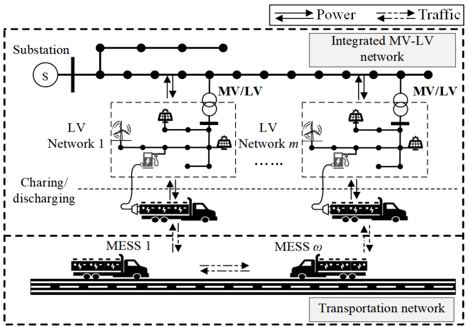

Fig. 1. An integrated MV-LV-transportation system with MESSs.

problem to find the improved system RES HC with the aid of MESS flexibility.

The remainder of this paper is organized as follows. Section II introduces the MESS scheduling model formulated based on the time-space network (TSN) model. Section III presents the detailed RES HC model for MV-LV networks. Case studies are given in Section IV and conclusions are drawn in Section V.

II. Mobile Energy Storage System Scheduling Model

A. System Model

Considering that MESSs are mainly scheduled to travel within the existing transportation networks to provide services to the facilities in the distribution system at different locations, besides distribution system models, a proper transportation network model is also essential. In this paper, an integrated MV-LV-transportation system is introduced to model the coordination among distribution systems and MESSs.

The general framework of an integrated MV-LV-transportation system is illustrated in Fig.1, which comprises two sub-systems, i.e., a transportation network and an integrated MV-LV distribution network, which is modeled as a graph with multiple subgraphs $\{\mathcal{G}_n := (\mathcal{V}_n, \mathcal{E}_n)\}_{n\in\mathcal{N}_{MV}\cup\mathcal{N}_{LV}}$, where $\mathcal{N}_{MV}$, $\mathcal{N}_{LV}$ are the sets of MV networks and LV networks, while $\mathcal{V}_n$, $\mathcal{E}_n$ are the sets of buses and distribution lines in the corresponding network *n*, respectively. Let $\mathcal{F}_{ML} : \mathcal{V}_{MV} \to \mathcal{P}(\mathcal{N}_{LV})$ be the mapping that maps each MV bus to the corresponding subset of LV networks connected to the bus, where $\mathcal{P}(\cdot)$ denotes the power set. These two networks are coupled together by a set of MESS stations $\mathcal{M}$, to which a set of MESSs defined by Ω can be connected, and their charging, and discharging behaviors at each station. Note that for simplicity only PV and WTs are considered in this paper.

B. TSN-based MESS Scheduling Model

To describe the detailed spatiotemporal behaviors of the MESSs within the integrated system, and enable the decision-making process, a TSN technique is adopted in this paper [11], [13]. Meanwhile, it is assumed that when traveling between two stations $\widehat{m}$, $\breve{m} \in \mathcal{M}$, MESS $\omega \in \Omega$ will always choose the path with the shortest distance in the transportation network that connects these stations. Let $l_{\widehat{m}\breve{m}}$ denote the length of this shortest path, which can be easily obtained by using many existing methods such as Dijkstra's algorithm, and each path is associated with a travel time $\tau_{\widehat{m}\breve{m}} = \lceil l_{\widehat{m}\breve{m}} / v_{avg}\Delta t \rceil, \forall \widehat{m}, \breve{m} \in \mathcal{M}$, indicating the number of time intervals required for ω to travel between $\widehat{m}$ and $\breve{m}$, where v_{avg} is the average speed of MESSs,

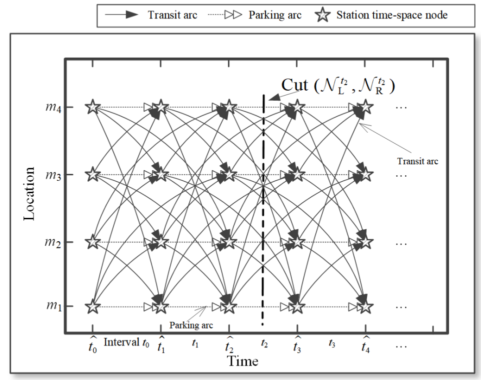

Fig. 2. Time space network model.

Δt is the length of each time interval and $\lceil\cdot\rceil$ is the ceiling function. Note that in this paper it is assumed that all the MESSs have the same average speed and Δt is set to be the same as the power system operation time scale. Also, let $\mathcal{T}$ denote the set of time intervals in the considered time horizon, indexed by *t*. Each time interval has two endpoints and let $\widehat{\mathcal{T}}$ be the set of these time points.

To better demonstrate the construction of the TSN model, consider a simple integrated MV-LV-transportation system with four LV networks, and each LV network is equipped with one MESS station. The complete TSN model for MESS scheduling is illustrated in Fig. 2, which consists of *1) Station time-space nodes* $\mathcal{N}_S = \{(m, \widehat{t}) \mid m \in \mathcal{M}, \widehat{t} \in \widehat{\mathcal{T}}\}$: represent the stations at specific time points; *2) Transit arcs* $\mathcal{A}_T$: a transit arc shows a feasible origin-destination pair of $\mathcal{N}_S$. For instance, arc $((m_1, \widehat{t_0}), (m_3, \widehat{t_2}))$ indicates that the MESS leaves m_1 at $\widehat{t_0}$ and reaches m_3 at $\widehat{t_2}$. *3) Parking arcs* $\mathcal{A}_P$: a parking arc connects two time-space nodes of the same station in a single interval, indicating that the MESS stays at the same station in a certain time interval, e.g., $((m_1, \widehat{t_0}), (m_1, \widehat{t_1}))$ claims that the MESS stays at m_1 during time interval t_0.

With the TSN model, the spatiotemporal scheduling decisions of MESSs can be represented by a sequence of the time-space arcs, where the formulations are based on arc-wise binary variables $\zeta^{\omega}_{\widehat{n}\breve{n}}$, which are 1 if MESS ω is on arc $(\widehat{n}, \breve{n}) \in \mathcal{A}_P \cup \mathcal{A}_T$. To facilitate the description of the MESS behavior using arcs and time-space nodes, a cut in each time slot *t* and the corresponding cut-set are also introduced [11].

With the definitions introduced, the TSN-based MESS scheduling model can be formulated as follows.

$$\sum_{(\widehat{n},\breve{n})\in\Phi_t} \zeta^{\omega}_{\widehat{n}\breve{n}} = 1, \forall \omega \in \Omega, t \in \mathcal{T} \tag{1}$$

$$\sum_{(\widehat{n},\breve{n})\in\overline{\mathcal{A}}_n} \zeta^{\omega}_{\widehat{n}\breve{n}} = \sum_{(\widehat{n},\breve{n})\in\overline{\overline{\mathcal{A}}}_n} \zeta^{\omega}_{\widehat{n}\breve{n}}, \forall n \in \mathcal{N}_S, \omega \in \Omega \tag{2}$$

$$\sum_{(\widehat{n},\breve{n})\in\overline{\mathcal{A}}_n} \zeta^{\omega}_{\widehat{n}\breve{n}} = \zeta^{\omega}_{ini}, \forall \omega \in \Omega \tag{3}$$

Equation (1) indicates that MESS ω can only be on one arc at each time slot. Constraints (2)-(3) refer to the flow conservation, i.e., each MESS ω ends its trip at time-space node *n* must stay on one of the arcs that start from node *n*, while ζ^{ω}_{ini} indicates the initial location of MESS ω. $\overline{\mathcal{A}}_n$, $\overline{\overline{\mathcal{A}}}_n$ are the sets of arcs that start from and end at time-space node *n*, respectively.

When staying on a parking arc, MESS ω is connected to the corresponding station and can provide energy services to the corresponding LV network. The relationship between its power/energy behavior and its temporal-spatial dynamics is constrained as follows.

$$0 \le P_{c,m}^{\omega,t} \le \zeta_{\hat{n}\check{n}}^{\omega} P_{c,\max}^{\omega}, \forall t \in \mathcal{T}, (\hat{n},\check{n}) \in \mathcal{A}_{P,m}^{t}, \omega \in \Omega, m \in \mathcal{M} \quad (4)$$

$$0 \le P_{d,m}^{\omega,t} \le \zeta_{\hat{n}\check{n}}^{\omega} P_{d,\max}^{\omega}, \forall t \in \mathcal{T}, (\hat{n},\check{n}) \in \mathcal{A}_{P,m}^{t}, \omega \in \Omega, m \in \mathcal{M} \quad (5)$$

$$0 \le \sum_{m\in\mathcal{M}} P_{c,m}^{\omega,t} \le I_{c}^{\omega,t} P_{c,\max}^{\omega}, \forall \omega \in \Omega, t \in \mathcal{T} \quad (6)$$

$$0 \le \sum_{m\in\mathcal{M}} P_{d,m}^{\omega,t} \le I_{d}^{\omega,t} P_{d,\max}^{\omega}, \forall \omega \in \Omega, t \in \mathcal{T} \quad (7)$$

$$I_{c}^{\omega,t} + I_{d}^{\omega,t} \le \sum_{m\in\mathcal{M}} \sum_{(\hat{n},\check{n})\in\mathcal{A}_{P,m}^{t}} \zeta_{\hat{n}\check{n}}^{\omega}, \forall \omega \in \Omega, t \in \mathcal{T} \quad (8)$$

$$E_{\omega}^{t} = E_{\omega}^{t-1} + \frac{\left(\eta_{c}^{\omega} \sum_{m\in\mathcal{M}} P_{c,m}^{\omega,t} - \sum_{m\in\mathcal{M}} P_{d,m}^{\omega,t} / \eta_{d}^{\omega}\right)\Delta t}{E_{\omega}^{\text{cap}}}, \quad \forall \omega \in \Omega, t \in \mathcal{T} \quad (9)$$

$$E_{\omega}^{\min} \le E_{\omega}^{t} \le E_{\omega}^{\max}, \forall \omega \in \Omega, t \in \mathcal{T} \quad (10)$$

where $P_{c,m}^{\omega,t}$, $P_{d,m}^{\omega,t}$ are the charging and discharging power output of MESS ω at station m in time interval t, while $P_{c,\max}^{\omega}$ and $P_{d,\max}^{\omega}$ are the maximum charging/discharging power allowed for MESS ω. $I_{c}^{\omega,t}$, $I_{d}^{\omega,t}$ are binary variables indicating whether MESS ω is performing charging or discharging in time interval t. E_{ω}^{t}, $E_{\omega}^{\max}$ and $E_{\omega}^{\min}$ are the current, maximum and minimum state-of-charge (SoC) of MESS ω.

Constraints (4) and (5) determine that represent the feasible power exchange behaviors between MESSs and stations, where $\mathcal{A}_{P,m}^{t}$ denotes the parking arcs of station m in time interval t. Constraints (6)-(7) indicate that each MESS can either perform charging or discharging in the same interval, which is co-constrained by its temporal-spatial behaviors as described in (8). Equation (9) illustrates the MESS SoC evolution while (10) ensures the SoC of MESS ω is within the desired range.

III. RES HOSTING CAPACITY ASSESSMENT WITH MESSS FLEXIBILITY

In this paper, the maximum RES HC of the integrated MV-LV distribution system is evaluated using an OPF-based framework, where the following operational constraints must be satisfied: 1) bus voltages must stay within the designed limits; 2) line flows must be constrained within their thermal capacities; 3) the reverse power flow through each LV transformer should not exceed the limit.

A. Objective Function

The objective function is to find the maximum RES HC for the integrated MV-LV distribution system considering MESS flexibilities, which is formulated as follows.

$$\max \sum_{i\in\bigcup_{n\in\mathcal{N}_{LV}}\mathcal{V}_n} \left(P_i^{\text{PV}} + P_i^{\text{WT}}\right) \quad (11)$$

where P_i^{PV} and P_i^{WT} are the PV and WT generation capacities to be installed on LV bus i.

B. Constraints

1) Constraints for the integrated MV-LV network: In this paper, the widely used branch flow model with conic relaxation is adopted for power flow analysis [14], and the detailed formulations are given as follows.

$$P_{G,j}^{n,t} + \sum_{m\in\mathcal{F}_{ML}(j)} P_{L2M}^{m,t} - P_{D,j}^{n,t} = \sum_{k\in\mathcal{V}_n} P_{jk}^{n,t} - \sum_{i\in\mathcal{V}_n} P_{ij}^{n,t}, \quad \forall j \in \mathcal{V}_n, n \in \mathcal{N}_{MV}, t \in \mathcal{T} \quad (12)$$

$$Q_{G,j}^{n,t} + \sum_{m\in\mathcal{F}_{ML}(j)} Q_{L2M}^{m,t} - Q_{D,j}^{n,t} = \sum_{k\in\mathcal{V}_n} Q_{jk}^{n,t} - \sum_{i\in\mathcal{V}_n} Q_{ij}^{n,t}, \quad \forall j \in \mathcal{V}_n, n \in \mathcal{N}_{MV}, t \in \mathcal{T} \quad (13)$$

$$P_{RES,j}^{n,t} - P_{L2M}^{n,t} + w_{PV}^{t} P_j^{\text{PV}} + w_{WT}^{t} P_j^{\text{WT}} + P_{MES,j}^{n,t} - P_{D,j}^{n,t} = \sum_{k\in\mathcal{V}_n} P_{jk}^{n,t} - \sum_{i\in\mathcal{V}_n} P_{ij}^{n,t}, \forall j \in \mathcal{V}_n, n \in \mathcal{N}_{LV}, t \in \mathcal{T} \quad (14)$$

$$-Q_{L2M}^{n,t} - Q_{D,j}^{n,t} = \sum_{k\in\mathcal{V}_n} Q_{jk}^{n,t} - \sum_{i\in\mathcal{V}_n} Q_{ij}^{n,t}, \quad \forall j \in \mathcal{V}_n, n \in \mathcal{N}_{LV}, t \in \mathcal{T} \quad (15)$$

$$P_{MES,j}^{n,t} = \sum_{m\in\mathcal{M}_j^n} \sum_{\omega\in\Omega} \left(P_{d,m}^{\omega,t} - P_{c,m}^{\omega,t}\right), \forall j \in \mathcal{V}_n, n \in \mathcal{N}_{LV}, t \in \mathcal{T} \quad (16)$$

$$V_j^{n,t} = V_i^{n,t} - 2(r_{ij} P_{ij}^{n,t} + x_{ij} Q_{ij}^{n,t}) + (r_{ij}^2 + x_{ij}^2) I_{ij}^{n,t}, \quad \forall j \in \mathcal{V}_n, n \in \mathcal{N}_{MV} \cup \mathcal{N}_{LV}, t \in \mathcal{T} \quad (17)$$

$$I_{ij}^{n,t} \ge \frac{P_{ij}^{n,t} + Q_{ij}^{n,t}}{V_i^{n,t}}, \forall (i,j) \in \mathcal{E}_n, n \in \mathcal{N}_{MV} \cup \mathcal{N}_{LV}, t \in \mathcal{T} \quad (18)$$

$$V_i^{n,t} = V_j^{m,t}, \quad \forall j \in \mathcal{V}_m^{\text{sub}}, m \in \mathcal{F}_{ML}(i), i \in \mathcal{V}_n, n \in \mathcal{N}_{MV}, t \in \mathcal{T} \quad (19)$$

$$\underline{P}_{L2M}^{n} \le P_{L2M}^{n,t} \le \overline{P}_{L2M}^{n}, \forall n \in \mathcal{N}_{LV}, t \in \mathcal{T} \quad (20)$$

$$\underline{Q}_{L2M}^{n} \le Q_{L2M}^{n,t} \le \overline{Q}_{L2M}^{n}, \forall n \in \mathcal{N}_{LV}, t \in \mathcal{T} \quad (21)$$

$$V_{i,\min}^{n} \le V_i^{n,t} \le V_{i,\max}^{n}, \forall i \in \mathcal{V}_n, n \in \mathcal{N}_{MV} \cup \mathcal{N}_{LV}, t \in \mathcal{T} \quad (22)$$

$$0 \le I_{ij}^{n,t} \le I_{ij,\max}^{n}, \forall (i,j) \in \mathcal{E}_n, n \in \mathcal{N}_{MV} \cup \mathcal{N}_{LV}, t \in \mathcal{T} \quad (23)$$

where $P_{ij}^{n,t}$, $P_{G,i}^{n,t}$, $P_{D,i}^{n,t}$, are the active power flow on branch (i, j), power generation and load on bus i in network n in time interval t, respectively. Note that in this paper unless otherwise specified, the similar symbols with Q represent the corresponding reactive power terms. $P_{L2M}^{n,t}$ is the active power injection to the MV network from LV network n through the corresponding MV/LV transformer, where negative values indicate that LV network n is withdrawing active power. $P_{RES,i}^{n,t}$, $P_{MES,i}^{n,t}$ are the existing RES generation and the aggregated MESS active power injected to bus i in LV network n in time interval t, while w_{PV}^{t} and w_{WT}^{t} are the normalized PV and wind profile in time interval t. $V_i^{n,t}$, $I_{ij}^{n,t}$ are the squared voltage and current magnitudes on bus i and branch (i, j), respectively.

Constraints (12)-(15) depict the active and reactive power balance equations at bus j for MV and LV networks, respectively. Equation (16) calculates the aggregated MESS output, where $\mathcal{M}_i^n$ denotes the set of MESS stations connected to bus i of LV network n. Constraints (17)-(18) depict the KVL

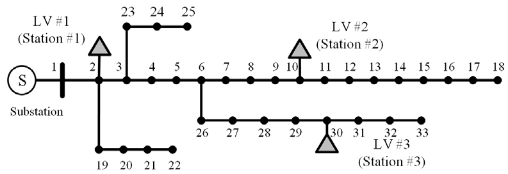

Fig. 3. A modified 33-bus MV test system with 3 LV networks.

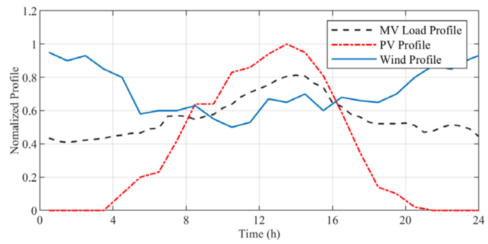

Fig. 4. Normalized MV load, PV and wind profiles.

with conic relaxation, while equation (19) illustrate the voltage coupling between MV buses and LV buses and $\mathcal{V}_m^{\text{sub}}$ is the substation bus. Note that we assume that $V_i^{n,t}$ stays at 1 at the MV substation. Finally, (20)-(23) represent the MV/LV transformer power limit, bus voltage limit and branch current limit, respectively.

2) Constraints for the integrated MV-LV network: besides constraints (12)-(23), TSN-based MESS scheduling constraints (1)-(10) are also included in the model.

IV. Case Studies

A. Test System

For simulations, an integrated MV-LV-transportation test system is introduced. This test system comprises a modified Sioux Falls transportation network with doubled link length, and an integrated MV-LV network, as shown in Fig. 3, which includes an IEEE 33-bus test system, where the voltage level is 12.66 kV and the peak load is 3.72 MW, 2.3 MVar [11], and three modified 18-bus test systems [15], where the system voltage level is reduced to 400V and the peak load is set to be 47.02 kW and 47.96 kVar. Within each LV network a MESS station is installed and connected to LV bus #2, i.e., station m_1, m_2 and m_3, and they are located at nodes #3, #19 and #24 in the transportation network, respectively.

It is assumed that LV network #1 only install new WTs while LV #2, #3 LV only install new PVs. LV bus #2, #5, #8, #12 and #17 are considered for RES installation. Also, LV networks #2 and #3 have already installed 30 kWp PV arrays at LV bus #10 #11 and #18, while the local loads in each LV network are of different types, i.e., industrial, commercial and residential, respectively, and the corresponding load profiles follow the load curves in [13]. The normalized MV load, PV and wind profiles are given in Fig. 4. The reverse power flow limit at MV/LV transformer is set to be 100 kW and 100 kVar, the bus voltage upper and lower limits are set to be 1.1 p.u. and 0.9 p.u., respectively, and the branch thermal limit is set based on a maximum current of 300A. In total, six MESSs are considered for the case studies, and their specifications are provided in Table I, and Δt is set to be 30 minutes.

Table I. Simulation Parameters

MESS#	$P_{\text{c,max}}^{\omega}$ (kW)	$P_{\text{d,max}}^{\omega}$ (kW)	E_{ω}^{cap} (kWh)	$\eta_{\text{c}}^{\omega}, \eta_{\text{d}}^{\omega}$	$\zeta_{\text{ini}}^{\omega}$
1	50	50	100	0.95	m_1
2	50	50	100	0.95	m_2
3	100	100	200	0.95	m_3
4	50	50	100	0.95	m_1
5	50	50	100	0.95	m_2
6	100	100	200	0.95	m_3

Table II. Numerical Results

Case #	LV #1 WT Capacity and bus #	LV #2 PV Capacity and bus #	LV #3 PV Capacity and bus #	Total RES HC
1	2.1 kW, #5 42.9 kW, #8 47.8 kW, #12 70.8 kW, #17	100.3 kW, #2	41.4 kW, #2 75.6 kW, #5	380.9 kW
2	10.6 kW, #2 3.2 kW, #5 90.3 kW, #8 58.9 kW, #12 79.2 kW, #17	4.8 kW, #2 53.9 kW, #8 30.9 kW, #12 46.5 kW, #17	2.9 kW, #2 29.5 kW, #8 25.9 kW, #12 37.8 kW, #17	474.4 kW

Two simulated cases are conducted and analyzed to verify the effectiveness of the MESSs serving as HC enhancements. Case 1: MESSs stay at their corresponding initial location and act as stationary ESSs; Case 2: MESSs are scheduled accordingly to fully utilize their spatiotemporal flexibilities. The model is implemented using Python 3.9 and solved using the off-the-shelve solver Cplex 12.8.0.

B. Simulation Results

The numerical results are presented in Table II. It can be observed that compared to Case 1, where the obtained total RES HC is 380.9 kW, the maximum RES HC obtained in Case 2 reaches 474.4 kW, which is increased by 24.5%. This is due to the additional operational flexibility introduced by the spatiotemporal mobility of the MESSs. As can be seen from the results that the improvements of HC are mainly located in LV #1. This is because that in LV #1, WTs are considered for newly installation. Due to the differences in wind and PV profiles, MESSs in LV #2 and #3 are firstly scheduled to move to LV #1 for wind HC enhancements during the first few hours where PV outputs are relatively low. After that, these MESSs are then scheduled to travel back to LV #2 and #3 for PV HC support. Meanwhile, due to the lack of mobility, stationary ESSs can only help to improve the system HC to some extent, considering their limited capacities.

Fig. 5 provides the charging and discharging schedules with respect to the MESS routing results for MESS #1 #2 and #3. As can be seen that the flexibility of MESSs is fully utilized to achieve maximum RES HC enhancement. For instance, MESS #2 initially travels from m_2 in LV #2 to m_1 in LV #1 during (0:00-1:00) and stays there during (1:00-2:00) to assist wind power integration. Then it leaves m_1 at 2:00, and arrive at m_3 in LV #3 at 2:30 to discharge and support the local loads. It repeats the similar behavior once again during (4:30-8:00). After that, as the PV generation is increasing in LV #2 and #3, MESS #2 then mainly move back and forth between these two LV networks for PV HC support. Similar behaviors can be observed for MESS #1 and #3. It is worth mentioning that unlike MESS #2, after sunset at around 20:00, these two MESSs again start to travel between m_1 and m_3 for wind HC enhancement.

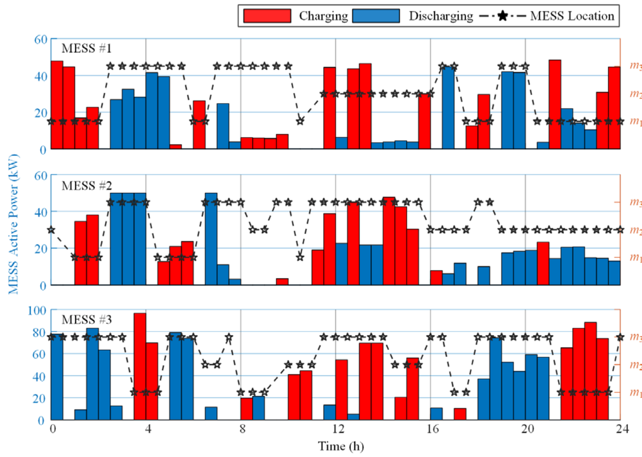

Fig. 5. MESS scheduling results.

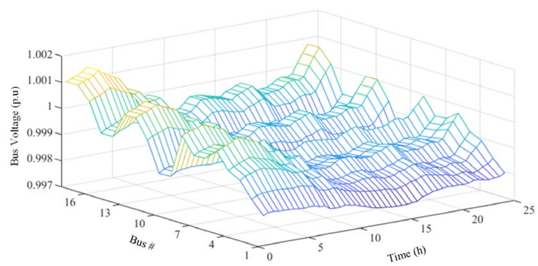

Fig. 6. Bus voltage profile of LV #1.

Fig. 6 illustrates the bus voltage profile in LV #1, it can be seen that no voltage violations occur and all bus voltages remain within a safe range in all time intervals. This is because that the main restriction of system HC in this case study is the power flow limitations for MV/LV transformers. Before obvious voltage rises are observed, the reverse power flow through the transformers will exceed their upper limits.

C. Practical and Policy Considerations

It should be clarified that this work aims to quantify the technical HC improvement enabled by exploiting MESS spatiotemporal flexibility. The related cost-benefit analysis is omitted here due to space limitation, and could be a future extension of this work. Still, a similar analysis can be referred to our previous work [11], which to certain extent validates the economic viability of utilizing MESSs for renewable energy accommodation. It is also worth noting that in certain counties such as China, RES utilization and integration is a mandatory operational indicator [16], while improving HC is an essential prerequisite for meeting these policy-driven requirements. This strengthens the practical motivation of studying the technical HC potential.

V. Conclusion

This paper studies the potential of MESSs serving as RES HC enhancements for integrated MV-LV systems. A TSN-based MESSs scheduling model is adopted for detailed description of MESSs' spatiotemporal flexibilities. Meanwhile, an OPF-based maximum RES HC evaluation model is formulated with the consideration of the couplings among the MESSs, MV, LV and transportation networks. Two cases are studied to verify the effectiveness of MESSs and their mobility to serve as potential RES HC enhancements and the results indicate that MESSs can achieve improved total system HC via their traveling between different networks and their charging and discharging behaviors at the corresponding MESS stations. Future works for this study could be further including local transportation networks for LV distribution systems, where a multi-layer TSN model can be introduced for MESS modeling. Moreover, uncertainties of RES outputs and transportation systems can be incorporated into the proposed model.

References

[1] International Energy Agency, "World Energy Outlook 2024," International Energy Agency, Tech. Rep., 2024. [Online]. Available: https://www.iea.org/reports/world-energy-outlook-2024

[2] B. Kroposki, B. Johnson, Y. Zhang, V. Gevorgian, P. Denholm, B.-M. Hodge, and B. Hannegan, "Achieving a 100% renewable grid: Operating electric power systems with extremely high levels of variable renewable energy," *IEEE Power and Energy Mag.*, vol. 15, no. 2, pp. 61–73, 2017.

[3] P. F. Lyons, P. Trichakis, R. Hair, and P. C. Taylor, "Predicting the technical impacts of high levels of small-scale embedded generators on low-voltage networks," *IET Renewable Power Generation*, vol. 2, no. 4, pp. 249–262, Dec. 2008.

[4] S. Hajeforosh, A. Khatun, and M. Bollen, "Enhancing the hosting capacity of distribution transformers for using dynamic component rating," *International Journal of Electrical Power & Energy Systems*, vol. 142, p. 108130, Nov. 2022.

[5] M. Bollen and F. Hassan, *Integration of Distributed Generation in the Power System*. Wiley, 2011.

[6] B. Currie *et al.*, "Flexibility Is Key in New York: New Tools and Operational Solutions for Managing Distributed Energy Resources," *IEEE Power and Energy Magazine*, vol. 15, no. 3, pp. 20–29, May 2017.

[7] S. M. Ismael, S. H. E. Abdel Aleem, A. Y. Abdelaziz, and A. F. Zobaa, "State-of-the-art of hosting capacity in modern power systems with distributed generation," *Renewable Energy*, vol. 130, pp. 1002–1020, Jan. 2019.

[8] N. Jayasekara, M. A. S. Masoum, and P. J. Wolfs, "Optimal Operation of Distributed Energy Storage Systems to Improve Distribution Network Load and Generation Hosting Capability," *IEEE Transactions on Sustainable Energy*, vol. 7, no. 1, pp. 250–261, Jan. 2016.

[9] L. H. Macedo, J. F. Franco, R. Romero, M. A. Ortega-Vazquez, and M. J. Rider, "Increasing the hosting capacity for renewable energy in distribution networks," in *2017 IEEE Power & Energy Society Innovative Smart Grid Technologies Conference (ISGT)*, IEEE, Apr. 2017, pp. 1–5.

[10] P. Astero and L. Söder, "Improving Hosting Capacity of Rooftop PVs by Quadratic Control of an LV-Central BSS," *IEEE Transactions on Smart Grid*, vol. 10, no. 1, pp. 919–927, Jan. 2019.

[11] X. Liu, C. B. Soh, T. Zhao, and P. Wang, "Stochastic Scheduling of Mobile Energy Storage in Coupled Distribution and Transportation Networks for Conversion Capacity Enhancement," *IEEE Transactions on Smart Grid*, vol. 12, no. 1, pp. 117–130, Jan. 2021.

[12] Z. Lin, C. Liu, H. Zhang, Z. Liu, and C. Chen, "Distributed Photovoltaic Location Planning and Hosting Capacity Improvement Considering Network Reconfiguration and Mobile Energy Storage," in *2023 IEEE 7th Conference on Energy Internet and Energy System Integration (EI2)*, IEEE, Dec. 2023, pp. 1901–1906.

[13] S. Yao, P. Wang, X. Liu, H. Zhang, and T. Zhao, "Rolling Optimization of Mobile Energy Storage Fleets for Resilient Service Restoration," *IEEE Transactions on Smart Grid*, vol. 11, no. 2, pp. 1030–1043, Mar. 2020.

[14] M. Farivar and S. H. Low, "Branch Flow Model: Relaxations and Convexification—Part I," *IEEE Transactions on Power Systems*, vol. 28, no. 3, pp. 2554–2564, Aug. 2013

[15] N. R. Battu, A. R. Abhyankar, and N. Senroy, "DG planning with amalgamation of economic and reliability considerations," *International Journal of Electrical Power & Energy Systems*, vol. 73, pp. 273–282, Dec. 2015.

[16] "China faces rising renewable energy curtailment." Accessed: Nov. 04, 2025. [Online]. Available: https://www.power-technology.com/news/china-renewable-energy-curtailment/

979-8-3315-8138-1